1 **Dynamical Model of Drug Accumulation in Bacteria: Sensitivity Analysis and**

2 **Experimentally Testable Predictions**

3

4 Neda Vesselinova[1,2], Boian S. Alexandrov[1], and Michael E. Wall*[3]

5

6 [1]Theoretical Division, Los Alamos National Laboratory, Los Alamos NM 87545

7 [2]University of California, Los Angeles, CA 90095

8 [3]Computer, Computational, and Statistical Sciences Division, Los Alamos National

9 Laboratory, Los Alamos NM 87545

10

11 *Corresponding author

12

13 August 8, 2016

14

15 LA-UR-15-28626

16   **Abstract.** We present a dynamical model of drug accumulation in bacteria. The

17   model captures key features in experimental time courses on ofloxacin

18   accumulation: initial uptake; two-phase response; and long-term acclimation. In

19   combination with experimental data, the model provides estimates of import and

20   export rates in each phase, the time of entry into the second phase, and the decrease

21   of internal drug during acclimation. Global sensitivity analysis, local sensitivity

22   analysis, and Bayesian sensitivity analysis of the model provide information about

23   the robustness of these estimates, and about the relative importance of different

24   parameters in determining the features of the accumulation time courses in three

25   different bacterial species: *Escherichia coli*, *Staphylococcus aureus*, and *Pseudomonas*

26   *aeruginosa*. The results lead to experimentally testable predictions of the effects of

27   membrane permeability, drug efflux and trapping (e.g., by DNA binding) on drug

28   accumulation. A key prediction is that a sudden increase in ofloxacin accumulation

29   in both *E. coli* and *S. aureus* is accompanied by a decrease in membrane permeability.

30

31   **Author Summary**. Bacteria live or die depending on how much antibiotic gets

32   inside them. Using a simple mathematical model, detailed information about drug

33   import and export can be teased out of time courses of internal drug levels after a

34   sudden exposure. The results suggest that membrane permeability can suddenly

35   decrease during exposure to drug, accompanied by an increase, rather than a

36   decrease, in the internal drug level.

37

38 **Introduction**

39

40 Drug resistance in bacteria can be increased by efflux pump systems [1], and pump

41 inhibition has emerged as a strategy for overcoming drug resistance [2]. Many

42 details of how efflux pumps work are still unclear, however. In particular,

43 quantitative information about how efflux influences drug accumulation in bacteria

44 is still scarce [3].

45

46 Drug accumulation is a key factor in obtaining a quantitative understanding of

47 resistance. For example, predictions of minimum inhibitory concentrations (MICs)

48 of β-lactams in *Escherichia coli* were obtained by equating the steady state

49 periplasmic drug concentration with a periplasmic binding protein inhibitory

50 concentration [4]. A predicted MIC was calculated as the *external* concentration that

51 would yield the accumulated *internal* inhibitory concentration in steady state,

52 considering flux terms from membrane permeation and β-lactamase degradation.

53 MIC predictions also have been made considering the action of efflux pumps on

54 cephalosporins [5] and β-lactams [6] in *E. coli*. These predictions were accompanied

55 by estimates of efflux pump kinetic constants (*i.e.*, K_m and V_{max} values), providing an

56 explicit connection between efflux and resistance.

57

58 Time-dependent drug accumulation studies also have yielded insight into drug

59 transport [7-9]. Diver et al. [8] found exposure of *E. coli* to five different quinolones

60 induced a rapid ~10 sec uptake followed by a ~30 min phase of more gradual

3

61   accumulation. Similar two phase behavior was seen by Asuquo and Piddock [7] in

62   accumulation of fifteen different quinolones in *E. coli*, *Pseudomonas aeruginosa*, and

63   *Staphylococcus aureus* [7]. The experiments of Asuquo and Piddock [7] highlighted

64   exposure to ofloxacin, which exhibited apparently different accumulation behavior

65   in each species (Fig. 1). Whereas drug levels appeared to plateau in *E. coli* (Fig. 1A)

66   and *S. aureus* (Fig. 1C) levels in *P. aeruginosa* gradually decreased at longer times

67   (Fig. 1B), suggesting an acclimation process.

68

69   Mathematical modeling has provided substantial insights into accumulation of β-

70   lactams [4,6], cephalosporins [5], and tetracycline [9] in *E. coli*. Quinolone

71   accumulation, however, has not yet been analyzed in the context of a mathematical

72   model. Here we present a mathematical model of drug accumulation and use it to

73   analyze experimental data on accumulation of the quinolone ofloxacin in *E. coli*, *S.*

74   *aureus*, and *P. aeruginosa* [7]. The analysis yields estimates of permeation and efflux

75   rates, the time of entry into the second phase of the response, and the rate of

76   decrease of drug during acclimation. We also perform global sensitivity analysis,

77   local sensitivity analysis, and Bayesian sensitivity analysis of the model. The

78   sensitivity analyses provide information about the robustness of parameter

79   estimates and enable assessment of the relative importance of the short-term

80   response and long-term acclimation in different bacterial species.

81

82   The results lead to experimentally testable predictions of membrane permeability

83   and drug efflux, which influence drug resistance. A key prediction is that an increase

84   in *E. coli* and *S. aureus* drug accumulation is accompanied by a decrease in

85   membrane permeability. Overall the results indicate the utility of mathematical

86   modeling and sensitivity analysis in obtaining new insights into drug accumulation

87   in bacteria.

88

89   **Results**

90

91   ***Model behavior***

92

93   Both the *E. coli* (Fig. 1A) and *P. aeruginosa* (Fig. 1B) behavior clearly show two

94   phases of drug accumulation dynamics, which is captured by our model of drug

95   accumulation (Methods). The model also allows for the possibility of acclimation in

96   the second phase; this was initially added to capture the longer-time (~10-60 min)

97   behavior of *P. aeruginosa* (Fig. 1b). Although *S. aureus* data initially appeared to

98   involve only one phase (Fig. 1C), the modeling and sensitivity analysis later revealed

99   a significant two-phase behavior, with acclimation.

100

101   The relationship between the model parameters and the model behavior is

102   illustrated in Fig. 2. After exposure at $t = 0$, the first phase begins, where cellular

103   antibiotic levels rise and relax toward an asymptotic value a_1. The relaxation in this

104   phase is exponential with rate β_1. At time $t = \tau$, the second phase begins, where

105   antibiotic levels may either rise or fall towards a new asymptotic value a_2. The

106   relaxation in this phase is initially dominated by exponential relaxation with rate β_2.

5

107   Later, acclimation can dominate the dynamics, specified by modulation of β_2 by the

108   factor $[1+ \delta(t- \tau)]$ (or, equivalently, modulation of α_2 by $[1+ \delta(t- \tau)]^{-1}$; see

109   Discussion). Together these features capture the full set of salient behaviors

110   exhibited by the experimental data on ofloxacin accumulation [7] (Fig. 2).

111

112   ***Parameter estimates***

113

114   Optimal parameter values were estimated by fitting the model to data on ofloxacin

115   accumulation in *E. coli*, *P. aeruginosa*, and *S. aureus*. The fits were performed

116   assuming the same measurement error for each data point within the same curve

117   (Methods). Reasonable fits were obtained for all datasets (Fig. 1), with an optimal

118   value of the goodness of fit χ^2/NDF of 0.98, 1.5, and 0.74 for *E. coli*, *P. aeruginosa*,

119   and *S. aureus*, respectively. Values of β_1, β_2, and τ for *E. coli* and *S. aureus* were

120   surprisingly similar (Table 1) given the visible differences between the two datasets

121   (Fig. 1); the parameter values for *P. aeruginosa* differed from the other two cases

122   (Table 1). *E. coli* exhibits two phases of accumulation with little apparent long-term

123   acclimation, consistent with the low value of δ. *P. aeruginosa* shows a stronger

124   acclimation response, corresponding to the higher value of δ. *S. aureus* exhibits a

125   degree of acclimation (δ) that is intermediate between *E. coli* and *P. aeruginosa*.

126

127   ***Sensitivity analysis results***

128

129   We applied three types of sensitivity analysis to the model: global sensitivity

130   analysis (GSA), local sensitivity analysis (LSA), and Bayesian sensitivity analysis

131   (BSA). The GSA yielded a fine-grained assessment of the importance of each

132   parameter in determining the model behavior at each time point. The LSA indicated

133   parameters that are responsible for the principal variations in the immediate

134   neighborhood of the optimal values. The BSA provided a detailed picture of the

135   shapes of probability distributions of parameters in a more extended range about

136   the optimum than for the LSA, including correlations that arise due to the nature of

137   the model equations. Semi-quantitative sensitivity rankings of parameters for each

138   case are presented in Supplementary Table S1; the detailed results are described

139   below.

140

141   **Global Sensitivity Analysis (GSA)**

142

143   GSA results were obtained using log-uniform prior distributions over the ranges in

144   Table 2. The results for *E. coli* (Fig. 3A,B) and *S. aureus* (Fig. 3E,F) are similar, due to

145   the identical priors (Table 2) and the similarity in the optimal parameter values for

146   these cases (Table 1). The "main effect" index (a.k.a. the first-order sensitivity index)

147   quantifies the contribution to the variance of the model of each parameter alone,

148   while averaging over variations in other parameters, whereas the "total effect" index

149   quantifies the change in the variance of the model caused by the investigated

150   parameter and its interactions with any of the other parameters (Methods). Both the

151   main effect and total effect are measured on a scale from 0 to 1 for each parameter.

152   As a reference for the following paragraphs, a_1 and a_2 correspond to the initial

153   steady-state level of antibiotic in the first and second phase; β_1 and β_2 correspond to

154   the relaxation rates at the entry into the first and second phase; τ is the time of entry

155   into phase 2; and δ is the rate constant associated with acclimation.

156

157   For *E. coli* and *S. aureus*, the main effect of a_1, a_2, and β_1 is high, and the main effect

158   of β_2, τ, and δ is low (Figs. 3A, 3E). The total effect of a_1, β_1, a_2, and τ is high, and the

159   total effect is low for β_2 (especially at later times) and δ (Figs. 3B, 3F). The total

160   effect of a_1 remains high at long times, despite being associated with the first phase;

161   this is because the prior for τ spans the entire range 0-3600 s, enabling the first

162   phase to extend to long times in the analysis.

163

164   For *P. aeruginosa*, the main effect of a_1, a_2, and δ is high, and the main effect of β_1, β_2,

165   and τ is low (Fig. 3C). The total effect of a_1, a_2, τ, and δ is high, and the total effect of

166   β_1 and β_2 is low (Fig. 3D). The increased importance of δ for *P. aeruginosa* compared

167   to *E. coli* and *S. aureus* is consistent with the more pronounced acclimation response

168   (Fig. 1). The low importance of β_1 and β_2 is consistent with the unbounded upper

169   limit due to the step-like transitions in *P. aeruginosa*; in comparison, the behavior of

170   *E. coli* and *S. aureus* shows more gradual relaxations with improved sampling (Fig.

171   1), leading to increased importance of β_1 and β_2 .

172

173   **Local sensitivity analysis (LSA)**

8

174   The LSA results are presented using the eigenvectors and eigenvalues of the

175   covariance matrix of model parameters (Methods). The eigenvectors are visualized

176   in columns of colored squares in Fig. 4, ordered in importance from left to right

177   using the eigenvalues (Table 3; sensitivity values correspond to -$\text{Log}_{10}(\lambda)$, where λ

178   is the eigenvalue). For all cases, the first two eigenvectors are dominated by a_1 and

179   a_2, indicating that these are the most sensitive parameters. For *E. coli*, the third

180   eigenvalue is more than 10-fold larger than the first eigenvalue (corresponding to a

181   lower sensitivity), with an eigenvector that is dominated by τ. The lowest

182   sensitivities correspond to combinations of β_1, β_2, and δ. For *P. aeruginosa*, the third

183   eigenvalue is 50-fold larger than the first, and corresponds to δ. The lowest

184   sensitivities correspond to β_1, β_2, and τ. For *S. aureus*, the third eigenvalue is 100-

185   fold larger than the first, and corresponds to β_1. The lowest sensitivities correspond

186   to combinations of β_1, δ, and τ. The relatively low sensitivity of τ in the LSA is

187   consistent with the very sharp transition between the two phases, as the precise

188   value of τ is ill-determined between the discretely sampled time points. The higher

189   sensitivity of τ for *E. coli* is consistent with the extrapolation of the phase 2

190   relaxation curve to a more precise value of τ.

191   **Bayesian sensitivity analysis (BSA)**

192   We used BSA with Markov Chain Monte Carlo (MCMC) sampling (Methods) to obtain

193   insight into probability distribution functions (PDFs) of parameter values (Figs. 5-7).

194   Because the measurement errors were not available for individual data points, we

195   used an arbitrary error of 1 ng/mg for each data point (Methods). The resulting

9

196   PDFs therefore should not be interpreted as actual posterior PDFs, but only as

197   indicators of: (1) the overall shape of the distributions; (2) the relative degree to

198   which different parameters are constrained; and (3) the relative degree and nature

199   in which different parameters are correlated.

200   The parameters β_1, β_2, and τ in *P. aeruginosa* have relatively flat PDFs that deviate

201   substantially from a normal distribution (Fig. 6). Sharpening the likelihood function

202   by decreasing the errors 10-fold led to sharper PDFs for peaked distributions

203   (Supplementary Figs. S1-S3) while maintaining similarly flat distributions for these

204   parameters (Fig. S2), providing evidence that the flat distributions are not an

205   artifact of the sampling.

206

207   The individual PDFs for the parameters of both *E. coli* (Fig. 5) and *S. aureus* (Fig. 7)

208   all show peaks, which is justification for the providing the estimates for all

209   parameters in Table 1 (the distribution of β_2 for *S. aureus* is truncated at low values

210   due to the restricted range of the prior; however, the peak clearly falls within the

211   range of the prior when the likelihood function is sharpened (Supplementary Figure

212   S3)). The range of the values of β_2 and δ among the MCMC sampled points (an

213   indicator of the width of the PDFs) is greater than for other parameters (Table 4),

214   indicating that estimates of β_2 and δ are less reliable (there is a noticeable tail in the

215   a_2 distribution for *E. coli*, but the range of 0.14 Log_{10} units is still sufficiently narrow

216   to provide an estimate). The pairwise scatter plots indicate relatively strong

217   correlations between a_2 and both β_2 and δ. These correlations follow from Eq. (4), in

10

218   which both β_2 and δ appear in factors that multiply a_2; a weaker correlation

219   between δ and β_2 is explained by the same term. The correlations involving δ are

220   only substantial when δ is sufficiently large; this is because the effect of δ is

221   negligible when it is smaller than about 10^{-5} s^{-1} (Eq. 4, considering the experiment

222   duration of 3600 s). In addition, β_1 appears in the term modulating a_1 in Eq. (4),

223   explaining a weak correlation between these two.

224

225   Like for *E. coli* and *S. aureus*, the PDFs of a_1, a_2, and δ for *P. aeruginosa* show peaks

226   (Fig. 6), justifying the entry of estimates in Table 1. In addition the PDF for τ,

227   although flat, is confined to a very narrow range, leading to an estimate in Table 1.

228   The lack of a peak for τ can be understood by the sharp, step-like increase (Fig. 1B)

229   combined with the discrete sampling in time; i.e., the step can be located anywhere

230   between the time points that mark the increase, with approximately equal

231   probability. Step-like increases in accumulation also lead to high uncertainty in both

232   β_1 and β_2 (Table 4); these parameters can assume essentially any value that is large

233   enough to enable the antibiotic to rise between the time points that mark the

234   increase, with equal probability. Like for *E. coli* and *S. aureus*, a_2 and δ are correlated

235   for *P. aeruginosa*; however, compared to *E. coli* and *S. aureus*, increased uncertainty

236   masks any underlying correlations involving β_1 and β_2.

237

238   ***Predictions of permeability, net efflux rate, and accumulation factor***

239   We used Eqs. (5)-(7) to predict the values of parameters that directly characterize

240   permeation, net efflux, and the degree of drug accumulation. The predictions are

241   quantified in the form of the permeability α_i in each phase i, the net efflux rate ε_i,

242   which is defined as the portion of the specific export rate not associated with

243   permeation, and the accumulation factor, ϕ_i, which is the fold-increase of antibiotic

244   concentration inside the cell compared to the external concentration. A positive

245   value of ε is associated with a net efflux and a value $\phi<1$, while a negative value is

246   associated with a net trapping of drug and a value $\phi>1$. The total value of ε can be

247   determined by a combination of individual positive or negative fluxes, potentially

248   involving multiple mechanisms including efflux pumps and drug binding to DNA

249   (Discussion).

250

251   The resulting predictions of α_i, ε_i, and ϕ_i are shown in Table 5. Predictions of α_i and

252   ε_i for *P. aeruginosa* are provided as lower bounds, following from the entries for β_i in

253   Table 1. The true reliability of the predictions of ϕ_i depends both on the robustness

254   of the estimation of a_i (Sensitivity analysis results) and the uncertainty in the factor

255   used to convert a_0 to ng/mg dry weight units (Methods). The reliability of the

256   predictions of α_i, ε_i additionally depends on the robustness of the estimation of β_i.

257   The predictions of permeability behavior are strikingly similar for *E. coli* and *S.*

258   *aureus.* At early times, the permeability is high, corresponding to about a 5.5 s half-

259   equilibration time for *E. coli*, and a 1.5 s half-equilibration time for *S. aureus* (α_1

260   from Table 5). The permeability then decreases dramatically after about 12.5

261   minutes (τ from Table 1): by a factor of ~50 for E. coli and a factor of ~100 for S.

262   aureus (α_2/α_1 from Table 5). In addition, the value of ε at both early and late times is

263   negative for both *E. coli* and *S. aureus*, and the values of ϕ are greater than one,

264   indicating a net trapping of antibiotic.

265   In contrast to *E. coli* and *S. aureus*, the values of ϕ are less than one for *P. aeruginosa*,

266   indicating a net efflux of antibiotic. The lower bound of α_1 for *P. aeruginosa* is

267   consistent with *E. coli* and *S. aureus* but the lower bound of α_2 is higher by a factor

268   O(10). The upper bounds of ε for *P. aeruginosa* are consistent with the estimates for

269   *E. coli* and *S. aureus.*

270   **Discussion**

271   The present modeling and analysis of ofloxacin accumulation time courses indicates

272   that *E. coli* and *S. aureus* exhibit a similar two-phase ofloxacin accumulation

273   behavior. Whereas the two-phase behavior for *E. coli* was easily visible in the data,

274   for *S. aureus* it was only detected as a result of the BSA. Even though the change in

275   antibiotic level entering phase 2 is small for *S. aureus*, the BSA indicates a clear peak

276   in the posterior distributions of all of the influx and outflux parameters, increasing

277   confidence in the two-phase model for this case (Fig. 7).

278

279   The contribution of sensitivity analysis to the present study was substantial. The

280   BSA enabled us to identify a significant two-phase model for *S. aureus* that we were

281   unable to detect in the data by eye. In addition, the BSA enabled us to identify

282   correlations in the data that are consistent with the way the parameters work

13

283   together in the model. We also note that the lack of individual error estimates for

284   each data point in the present study prevented calculation of true posterior PDFs;

285   the availability of error estimates for future datasets will enable a substantial

286   increase in the information provided by the BSA. The sensitivity analysis also

287   enables a quantitative means of distinguishing of important from unimportant

288   parameter values in the modeling. This further enables a degree of confidence to be

289   associated with results based on the quantitative analysis, which can be used to

290   assess which predictions are more or less likely. Some aspects of the sensitivity

291   analysis confirm what is already apparent in just looking at the data, such as the

292   increased importance of δ for *P. aeruginosa* compared to *E. coli*; however, even in

293   this case, it provides quantitative measures that can enable obvious results to be

294   obtained automatically. Automation will become increasingly important as we

295   increase the number of data sets being analyzed. In addition, future data sets might

296   not be as straightforward to interpret by eye, and the present study serves as an

297   example that demonstrates the consistency of the sensitivity analysis with the

298   interpretation of a relatively clear-cut case, so that the methods can be applied with

299   increased confidence to cases where the interpretation might not be so obvious.

300

301   The rapid initial accumulation of ofloxacin in *E. coli*, *P. aeruginosa*, and *S. aureas* has

302   been cited as evidence that these bacteria lack a substantial permeability barrier for

303   fluoroquinolones [7]. Our modeling supports the high permeability at early times in

304   the accumulation dynamics. The permeation rates in Table 5 lead to a half-

305   equilibration time for ofloxacin permeation of 5.5 s into *E. coli*, <18 s into *P.*

14

306   *aeruginosa*, and 1.5 s for *S. aureus*. These values are similar to the expected 5 s half-

307   equilibration time for permeation of norfloxacin across a lipid bilayer [10]; as

308   measured in Ref. [7], the apparent partition coefficient of ofloxacin is 4-fold greater

309   than that of norfloxacin, so their permeabilities across the cytoplasmic membrane

310   are expected to be within a similar range.

311   In contrast with the early time behavior, after about 12.5 mins, both *E. coli* and *S.*

312   *aureus* show a predicted 50-to-100-fold decrease in permeability (Table 5). This

313   sudden decrease in permeability only was detected using the modeling and was not

314   detected in the prior qualitative analysis of the data [7]. One way to test this

315   prediction is to shift the cells to a medium with radiolabeled drug, looking for a

316   difference in labeled drug accumulation in phase 1 versus phase 2. At this point we

317   can only speculate about the mechanism. *E. coli* is gram negative, whereas *S. aureus*

318   is gram positive, suggesting the common decrease in permeability does not involve

319   the outer membrane. That the permeability rates are consistent with diffusion

320   across the cytoplasmic membrane indicates that the decrease in permeability is not

321   necessarily be associated with transporters. It is possible that the sacculus, a mesh

322   structure common to both *E. coli* and *S. aureus*, might be involved in a decrease in

323   permeability. The ability of the sacculus to allow translocation of proteins as large as

324   25 kDa [11] or 100 kDa [12] would seem to rule out a role for the sacculus by itself,

325   as ofloxacin has a molecular weight of 361 Da, and should ordinarily freely diffuse

326   across the mesh. However, the sacculus is associated with a comparable mass of

327   other biomolecules in both gram negative and positive bacteria [13] [14]. If ~98%

328   of the mesh were to become blocked somehow, it could explain the ~50-fold

15

329   decrease in permeability for *E. coli*.

330   For *E. coli* and *S. aureus*, the values of the accumulation factor $\phi > 1$ indicate net

331   trapping of antibiotic. The trapping is weak for *E. coli* in phase 1 ($\phi_1 = 1.09$) and

332   becomes stronger in phase 2 ($\phi_2 = 2.29$). Compared to *E. coli*, the trapping is stronger

333   in *S. aureus* for both phases: $\phi_1 = 2.93$ and $\phi_2 = 3.75$. For *P. aeruginosa*, the values of

334    $\phi < 1$ indicate a net efflux of antibiotic that is stronger in phase 1 ($\phi_1 = 0.39$) than in

335   phase 2 ($\phi_2 = 0.72$).

336

337   Several individual effects can combine to determine whether there is a net trapping

338   or efflux of antibiotic. Targeted experiments will be required to determine the role

339   of specific mechanisms, but we can gain some insights by assuming that an

340   important effect favoring trapping is the immobilization of antibiotic on DNA. This

341   effect can be estimated using the dissociation constant $K_D = 633$ μM reported by

342   Shen et al. [15] for nonspecific binding to DNA of norfloxacin at high concentrations

343   (10-1000 μM). Assuming roughly 2.1 genome equivalents per cell [16], a volume of

344   1.25 fL, and 4.7×10^6 bp per chromosome yields an estimated DNA bp concentration

345   in *E. coli* [D] $= 1.3 \times 10^4$ μM. Then, assuming the K_D for norfloxacin applies to

346   ofloxacin and that each bp can bind one drug molecule yields a fraction of DNA-

347   bound drug of $1/(1+K_D/[D]) = 0.95$, or a mobile fraction of just 0.05. In this case, the

348   contribution of permeability to the outflow would be only 5% of that assumed in Eq.

349   (6), leading to an increase in efflux by 0.95α. This translates into an increase in the

350   specific efflux rate by 0.12 s^{-1} for *E. coli* in phase 1.

16

351   Based on the above estimates, despite the small negative value of the net efflux

352   parameter ε_1 (= -0.011 s^{-1}) in Table 5, due to the effect of trapping by DNA binding,

353   we expect the underlying rate of efflux in *E. coli* to be 0.11 s^{-1} (= 0.12 s^{-1} - 0.011 s^{-1}),

354   which is comparable to the rate of permeation. To assess the importance of efflux in

355   *S. aureus*, we use similar reasoning as for *E. coli*, noting that the net efflux parameter

356   ε_1 is -0.326 s^{-1} and the effective permeability α is 0.495 s^{-1} (Table 5). Assuming the

357   same degree of trapping in *S. aureus* as in *E. coli* yields a contribution 0.48 s^{-1} and an

358   estimated specific efflux rate of roughly 0.15 s^{-1} (= 0.48 s^{-1} - 0.326 s^{-1}) in phase 1,

359   which is close to the value for *E. coli*. In contrast to *E. coli*, however, where the efflux

360   rate is comparable to the inflow rate, in *S. aureus* the efflux rate is less than 1/3 of

361   the inflow rate.

362   The estimated specific efflux rates in phase 1 of 0.11 s^{-1} for *E. coli* and 0.15 s^{-1} for *S.*

363   *aureus* can be used to estimate the rate of outflow of drug due to efflux. Multiplying

364   by a_1 yields an outflow of 3.5 ng/mg/s (= 0.11 s^{-1} x 32 ng/mg) for *E. coli*, and 10

365   ng/mg/s (= 0.15 s^{-1} x 66.6 ng/mg) for *S. aureus*. Dividing by the molecular weight of

366   ofloxacin (361.368 g/mol) yields 0.0097 nmol/mg/s for *E. coli* and 0.028

367   nmol/mg/s for *S. aureus*. These values are similar to the V_{max} value of 0.0235 ± 0.003

368   nmol/mg/s found by Lim and Nikaido [6] for efflux of nitrocefin from *E. coli*, and are

369   much lower than the value of 1.82 ± 0.85 nmol/mg/s found for cephaloridine efflux

370   from *E. coli* in the same study. Therefore our predictions are consistent with the V_{max}

371   for efflux of ofloxacin in *E. coli* and *S. aureus* being similar to the V_{max} for efflux of

372   nitrocefin in *E. coli*.

17

373   In addition to DNA binding, differential permeability of ionic subspecies of ofloxacin

374   or Mg2+ chelates of ofloxacin might also influence the balance of inflows and

375   outflows [10]. These effects can easily lead to two-fold or greater accumulation or

376   exclusion of antibiotic [10]. In addition to the predicted change in membrane

377   permeability, therefore, changes in DNA binding, efflux, pH, and the availability of

378   Mg2+ all might potentially be linked to the two-phase behavior of ofloxacin

379   accumulation.

380   Because we predict that the underlying efflux rate is comparable to the inflow rate

381   in *E. coli*, we also predict that efflux plays an important role in ofloxacin

382   accumulation. In contrast, for *S. aureus*, we predict efflux plays a less important role

383   in ofloxacin accumulation, because the efflux rate is predicted to be substantially

384   lower than the inflow rate. For *P. aeruginosa*, we are unable to make predictions

385   based on quantitative estimates of rate constants, due to uncertainty in the key

386   parameter values in Table 1 and Table 5. However, because the internal

387   concentration of antibiotic is predicted to be less than the external concentration (ϕ

388   < 1 in Table 5), we predict that efflux is important in *P. aeruginosa* accumulation of

389   ofloxacin.

390   Both *P. aeruginosa* and *S. aureus* exhibit a visible slow decrease in accumulated drug

391   during the second phase (Fig. 1). The model captures this decrease in terms of the

392   parameter δ which increases β_2 by a factor $[1 + \delta(t - \tau)]$ in Eq. (3). Mechanisms for

393   increasing β include enhancing efflux (e.g., by increased expression of pumps) or

394   decreasing trapping (e.g., by chromosome remodeling that results in a decrease in

18

395   drug binding to DNA). Importantly, the combination of Eq. (4) and Eq. (5) indicate

396   that δ can be interpreted alternatively as decreasing α_2 by a factor $[1 + \delta(t - \tau)]^{-1}$.

397   Thus, in addition to an increase in efflux or a decrease in trapping, the acclimation

398   behavior can be attributed to a decrease in permeability (e.g., through the

399   hypothetical mechanisms described above). Additional experiments targeted at the

400   mechanism of decrease will be required to determine the cause of the acclimation

401   response.

402

403   Ofloxacin is bactericidal at the concentration of 10 mg/L used in the experiments [7],

404   which might have important implications for the interpretation of the results. If

405   nonviable cells are excluded from the analyzed pellet after centrifugation (e.g.

406   because they have been lysed and remain suspended), the accumulation data simply

407   correspond to viable cells, and the interpretation is straightforward. If nonviable

408   cells are included in the pellet, the interpretation depends on the relative

409   populations of viable and nonviable cells. According to Ref. [7], 5 mins after

410   exposure in phosphate buffer, the viable count of *E. coli* decreased by 0.74 Log_{10}

411   units, the count of *P. aeruginosa* decreased by 0.45 Log_{10} units, and the count of *S.*

412   *aureus* decreased by 0.4 Log_{10} units. These data indicate that in all cases, the number

413   of viable cells decreases by at least 2.5-fold after 5 mins. At the longest times, 60

414   mins after exposure, the values were 2.06, 3.75, and 0.54 Log_{10} units, respectively,

415   indicating that the number of viable cells of *E. coli* and *P. aeruginosa* decreases by at

416   least 100-fold over the course of the experiment. These results indicate that if

417   nonviable cells are included in the analyzed pellet, the behavior should be

19

418   dominated by the nonviable cells; indeed, trapping of antibiotic in nonviable cells

419   removes antibiotic from the environment and can increase the chance of survival of

420   neighboring viable cells, leading to a fitness advantage at the population level.

421

422   That the model matches the data well (Fig. 1) is consistent with the interpretation

423   that the behavior is predominantly due to one type of cell, either viable or nonviable.

424   However, the killing kinetics do indicate that the number of viable cells is still not

425   negligible at early times for all cells, and at late times for *S. aureus*. In addition,

426   including the effect of antibiotic on cell growth and death will be critical to

427   connecting the present results to drug resistance. Future work should therefore

428   include investigating an expanded dynamical model that includes subpopulations of

429   viable and nonviable cells, including the dependence of cell growth (for

430   bacteriostatic effect) and death (for bactericidal effect) on intracellular antibiotic

431   concentration. Including the antibiotic effect (e.g., via the target inhibitory

432   concentration [4-6]) is essential for understanding the relation between the amount

433   of accumulated drug and antibacterial activity, as they are not necessarily correlated

434   [7]. In particular, Nagano and Nikaido [5] used mathematical modeling to predict

435   MIC values of drugs for *E. coli*, and to show how efflux pump deletion or

436   overexpression might not change the MIC value of drugs that are nevertheless

437   strong efflux pump substrates.

438

439   It is interesting to consider the importance of models of drug accumulation in light

440   of a recent survey of physical properties of active compounds in a drug screening

441   collection and their relation to whole cell antibacterial activity [17]. The survey

442   reported on the difficulties encountered in simultaneously optimizing both

443   biochemical potency and antibacterial activity, and concluded that "what is clearly

444   needed is greater insight into medicinal chemistry strategies which optimize

445   transport through porins and decrease efflux through the prolific efflux pumps."

446   Together, the findings reported here and elsewhere [5,6] suggest that mathematical

447   modeling of drug accumulation can provide these insights, and thus can be a key

448   tool in enabling antibacterial medicinal chemistry.

449

450   **Materials and Methods**

451

452   ***Model***

453

454   Our dynamical model of drug accumulation lumps together transport across the

455   inner and outer membranes. This is appropriate as the drug target is in the

456   cytoplasm, there are no data on drug accumulation in the periplasm, and we wish to

457   use the same model for gram positive or negative bacteria. We note that this

458   lumping does not prevent the interpretation of results in light of differences

459   between the outer and inner membranes (Discussion).

460

461   The time dependence of accumulated drug $a(t)$ is modeled using

462

21

$$\frac{da(t)}{dt} = \alpha(t)a_o - \beta(t)a(t) \qquad\qquad (1)$$

463

464 where a_o is the environmental antibiotic concentration, $\alpha(t)$ is the specific rate of

465 increase, and $\beta(t)$ is the specific rate of decrease. The term "specific" is used to

466 indicate that the rate constant is multiplied by the antibiotic concentration. We

467 assume $\alpha(t)$ corresponds to the permeability, although it also can include active

468 transport. We assume $\beta(t)$ corresponds to both active and passive transport,

469 although it also can include degradation and cell growth. Cell growth in *E. coli* occurs

470 by a constant cell size extension [18], which is consistent with including cell growth

471 in β. If included, assuming a 42 min doubling time, cell growth would contribute a

472 specific rate of 2.75×10^{-4} s^{-1}; this is orders of magnitude smaller than the values of

473 β at early times (Table 1), when growth is expected to be highest, and is at least 4-

474 fold smaller than the values of β at early times (Table 1), when growth is expected to

475 be lowest. Ignoring cell growth therefore is a reasonable approximation in the

476 present study, although it might be necessary to include it in other studies.

477

478 Equation (1) was developed assuming that only viable cells are analyzed. This

479 corresponds to the case when nonviable cells are disrupted and are excluded from

480 pellet after centrifugation in Ref. [7]. Even when nonviable cells are not excluded

481 from analysis (Discussion), Eq. (1) applies to viable cells when the external

482 antibiotic level is low and there is a negligible fraction of nonviable cells at all times.

483 If nonviable cells are included in the pellet and there is a negligible fraction of viable

484 cells at all times, Eq. (1) will still be relevant but will instead describe accumulation

22

485   in the nonviable cells. If both viable and nonviable cells are analyzed and there is an

486   intermediate drug concentration, the model should be extended to include both

487   viable and nonviable cells, with population dynamics (Discussion).

488

489   To model the data in Fig. (1), we assume α(t) and β(t) both switch rapidly from a

490   constant value in phase 1 to a different constant value in phase 2. The import rate

491   α(t) is given by

492

$$\alpha(t) = \begin{cases} \alpha_1, & t < \tau \\ \alpha_2, & t \geq \tau \end{cases} \qquad\qquad (2)$$

493

494   where α_1 applies to the early phase of the accumulation dynamics (t<τ), and α_2

495   applies to the late phase (t ≥ τ).

496

497   The export rate β(t) is given by

498

$$\beta(t) = \begin{cases} \beta_1, & t < \tau \\ \beta_2[1 + \delta(t - \tau)], & t \geq \tau \end{cases} \qquad\qquad (3)$$

499

500   where β_1 applies during the early phase (t<τ), β_2 applies during the late phase (t≥τ),

501   and δ is the fractional rate of increase of export during the later phase.

502

503   Assuming rapid relaxation (β_2) compared to acclimation (δ) in phase 2 yields

504

23

$$a(t) = \begin{cases} e^{-\beta_1 t}a(0) + \left(1 - e^{-\beta_1 t}\right)a_1, & t \leq \tau \\ e^{-\beta_2(t-\tau)}a(\tau) + \left[1 - e^{-\beta_2(t-\tau)}\right]\dfrac{a_2}{1 + \delta(t - \tau)}, & t > \tau \end{cases} \tag{4}$$

505

506   where $a_1 = \alpha_1 a_o / \beta_1$, and $a_2 = \alpha_2 a_o / \beta_2$.

507

508   Given additional assumptions, the α and β parameters can be used to derive

509   permeation and net efflux rates (see below). The δ parameter models long-term

510   acclimation by, e.g., gene regulation.

511

512   ***Parameter estimation***

513

514   Parameter estimation for Eq. (4) was performed using published experimental time

515   courses of ofloxacin accumulation in *E. coli*, *P. aeruginosa*, and *S. aureus* [7]. Data

516   points were extracted from Figure 1 in Ref. [7]. Numerical solutions to Eq. (4) were

517   obtained for each data point using functions defined in Mathematica Version 10

518   (Wolfram Research, Inc., Champaign, IL). Errors for each individual data point were

519   not available, and were therefore estimated using the maximum values given for

520   norfloxacin in Ref. [7]: ±12.5, ±11.6, and ±9.7 ng/mg for *E. coli*, *P. aeruginosa*, and *S.*

521   *aureus*, respectively. To obtain error estimates for ofloxacin, these maximal errors

522   were scaled using the initial rapid phase concentration entries in Tables II, III, and

523   IV of Ref. [7], and were then divided by two. The following were the resulting

524   estimated errors for each data point: 2.3 ng/mg for *E. coli*, 0.75 ng/mg for *P.*

525   *aeruginosa*; and 4.35 ng/mg for *S. aureus*. We also performed the fits using the

24

526   maximal errors as the estimates, without dividing by two; however, we favored

527   using the half-maximal errors for the following reasons: (1) the maximal values are

528   very likely overestimates; and (2) the half-maximal values yielded χ^2/NDF values

529   close to 1, whereas the maximal values yielded values substantially lower than 1.

530   The choice of errors between these cases merely resulted in a different overall

531   scaling χ^2 and did not influence the optimal parameter values obtained in the fits.

532

533   A standard χ^2/NDF was used as a goodness of fit measure between the model and

534   the data, using a number of degrees of freedom NDF = number of data points minus

535   six parameters. The χ^2/NDF was minimized with respect to values of a_1, a_2, β_1, β_2, δ,

536   and τ using the `FindMinimum` method, assuming a(0)=0. The values of a_1, a_2, β_1, β_2,

537   δ were varied over twelve decades. For *E. coli* and *P. aeruginosa*, the value of τ was

538   varied from 0-10,000 s (covering the full span of each 3,600 s time course) to seek

539   an optimal solution. For *S. aureus*, optimization was initially performed for τ =

540   10,000 s (a time beyond the last data point), as the behavior appeared to be one

541   phase. A more thorough investigation of the parameter space using Bayesian

542   sensitivity analysis (BSA), however, revealed a relatively weak but significant two-

543   phase response, with a value of τ that is similar to *E. coli*. Therefore the optimization

544   for *S. aureus* also was performed varying τ from 0-10,000 s. Mathematica

545   workbooks and experimental data for all cases are available in a compressed

546   archive in the Supporting Information.

547

548   ***Sensitivity analysis methods***

25

549

550   All sensitivity analyses were performed using the open source code Model-Analysis

551   and Decision Support (MADS), developed at Los Alamos National Laboratory

552   (http://mads.lanl.gov).

553

554   *Global Sensitivity Analysis (GSA)*: We performed variance-based GSA [19], which

555   decomposes the variance of the output into parts ascribed to different input

556   parameters using a Fourier Haar decomposition [20,21]. Both the "main effect " and

557   the "total effect" results presented here for each input parameter were calculated

558   using the Sobol Monte Carlo algorithm [22] using about 10^6 independent model

559   evaluations drawn from log-uniform distributions defined by Table 2. We found that

560   this number of samples was sufficient to achieve convergence for the estimated

561   quantities. The ranges in Table 2 were chosen arbitrarily to encompass the optima

562   in Table 1 while exploring a reasonably broad region of parameter space and

563   satisfying the requirement of rapid relaxation (β_2) compared to acclimation (δ) in

564   phase 2 for Eq. (4).

565

566   *Local Sensitivity Analysis (LSA)*: LSA has a rich history of use in assessing the

567   robustness of biochemical network model behavior to changes in parameter values

568   [23,24]. In LSA, the local gradients of the model output are calculated with respect

569   to model parameters at a fixed point (the point with the lowest χ^2). Here we use the

570   gradients to define a covariance matrix of variations [25]. We used a finite

571   difference method requiring a limited number of model evaluations (equal to the

26

572   number of unknown parameters). As a result, we obtain a gradient matrix **J** (i.e. the

573   Jacobian) with dimensions $[m \times n]$ where m is the number of model parameters and

574   n is the number of model inputs (we use logarithmic derivatives, to obtain an

575   analysis in terms of dimensionless parameters). Each component of the **J** matrix

576   represents the local sensitivity of each model parameter to each model output [25].

577   We analyze the covariance matrix **C** of model parameters which is computed as **C** =

578    $[J^TJ]^{-1}$. The covariance matrix is analyzed using eigenanalysis where eigenvectors

579   and eigenvalues of the covariance matrix are explored. How dominant (important)

580   is each eigenvector depends on the respective eigenvalues; the smaller the

581   eigenvalue, the higher the importance of the eigenvector. The components of each

582   eigenvector represent the contributions of each model parameter to the

583   simultaneous variation of multiple parameters: the larger the absolute value of the

584   components, the larger the contribution. Model parameters with a large

585   contribution in dominant eigenvectors are important (sensitive) model parameters.

586   Model parameters with large contribution in non-dominant eigenvectors are

587   unimportant (insensitive) model parameters. If several model parameters have an

588   important contribution in a single eigenvector, these model parameters are

589   correlated. If these contributions have the same sign, the correlation is positive. If

590   these contributions have opposite signs, the correlation is negative.

591

592   *Bayesian Sensitivity Analysis (BSA)*: Posterior probability density functions (PDFs) of

593   the model parameters given observed data (Figs. 5-7) were obtained following

594   Bayes' theorem [26,27]. The PDFs were obtained using a log-uniform prior with the

595   ranges indicated in Table 2, with a likelihood function defined as $e^{-\chi^2/2}$, using an

596   arbitrary error value of 1 ng/mg for each data point. The error was decreased to 0.1

597   ng/mg to demonstrate the effect of sharpening the likelihood function in

598   Supplementary Figs. S1-S3. The BSA was performed using the Robust Adaptive

599   Metropolis Markov Chain Monte Carlo (MCMC) algorithm [28]. Analysis was

600   performed using sample sizes of 10^4, 10^5, and 10^6; we found a sample size of 10^6

601   yielded adequate sampling. The posterior PDF scatter plots (off-diagonal panels in

602   Figs. 5-7) show an overlay of individual counts; the extent of the plots reflects the

603   parameter range over which 10^6 random samples can fall. The posterior parameter

604   ranges in Table 4 were obtained by identifying the minimum and maximum

605   parameter values among 10^6 points sampled using the MCMC. (The values in Table 4

606   must be interpreted in light of the fact that the range might increase with increasing

607   number of samples, and that the precise values can change depending on differences

608   in sampling, e.g., using different random number seeds.) The histograms (diagonal

609   panels in Figs. 5-7) indicate the shape of the individual marginalized PDFs using the

610   number of counts on the y-axis.

611

612   ***Predictions of permeability, net efflux rate, and accumulation factor***

613

614   Estimation of the model parameters enables prediction of permeability and efflux

615   rates. Given a_o, the specific import rate α_i in each phase *i* may be calculated as

$$\alpha_i = a_i \beta_i / a_0. \tag{5}$$

616

617 Assuming the import is due to permeation, α_i is the permeability. Next, assume the

618 specific export rate β is a sum of contributions from permeability, α and other

619 effects. The other effects are then captured by the difference ε between β and α:

620

$$\varepsilon_i = \beta_i - \alpha_i. \tag{6}$$

621

622 When $\varepsilon_i > 0$, outward flow is enhanced compared to permeation, and ε_i indicates a net

623 efflux. When $\varepsilon_i < 0$, the outward flow is decreased compared to permeation, and ε_i

624 indicates a net trapping of drug.

625

626 Finally, the accumulation factor ϕ is used as a measure of the degree to which

627 antibiotic is either accumulated in or expelled from the cell. It is given by

628

$$\phi_i = a_i / a_o. \tag{7}$$

629

630 If $\phi_i < 1$ the internal antibiotic concentration is less than the external antibiotic,

631 which is associated with net efflux ($\varepsilon_i > 0$). If $\phi_i > 1$ the internal antibiotic exceeds

632 the external antibiotic, which is associated with net trapping ($\varepsilon_i < 0$).

633

634 Eqs. (5)-(7) are only valid under the same assumptions as for Eq. (4). Predictions of

635 α_i and ε_i are only meaningful using reliable estimates of both a_i and β_i. In contrast,

636 ϕ_i can be predicted just with estimates of a_i and a_o.

637

29

638   The predictions use the environmental drug concentration a_0 in ng drug/mg dry

639   weight units. The external ofloxacin concentration in the experiments was 10 mg/L

640   [7]. To convert to ng/mg dry weight units, following Ref. [29], we used a buoyant

641   density of 1.1 g/mL and a 31% dry weight for *E. coli*, a buoyant density of 1.2 g/mL

642   and a 48% dry weight for *P. aeruginosa* (transferred from *P. putida*), and assumed a

643   buoyant density of 1.1 g/mL and a 40% dry weight for *S. aureus*. This yielded

644   conversion factors of 0.341 (mg drug/L)/(ng drug/mg dry weight) for *E. coli*, 0.528

645   for *P. aeruginosa*, and 0.440 for *S. aureus*. The uncertainty in the dry weight fraction

646   for *S. aureus* should be estimated at about 25%, given the range spanned by *E. coli*

647   and *P. aeruginosa*. This introduces uncertainty in the predictions beyond those

648   indicated by the sensitivity analysis alone.

649

650   **Acknowledgments**

651

657

658   **References**

659

660   1. Li XZ, Nikaido H (2009) Efflux-mediated drug resistance in bacteria: an update.
661   Drugs 69: 1555-1623.

30

662   2. Kourtesi C, Ball AR, Huang YY, Jachak SM, Vera DM, et al. (2013) Microbial efflux
663   systems and inhibitors: approaches to drug discovery and the challenge of
664   clinical implementation. Open Microbiol J 7: 34-52.
665   3. Nikaido H, Pages JM (2012) Broad-specificity efflux pumps and their role in
666   multidrug resistance of Gram-negative bacteria. FEMS Microbiol Rev 36: 340-
667   363.
668   4. Nikaido H, Normark S (1987) Sensitivity of Escherichia coli to various beta-
669   lactams is determined by the interplay of outer membrane permeability and
670   degradation by periplasmic beta-lactamases: a quantitative predictive
671   treatment. Mol Microbiol 1: 29-36.
672   5. Nagano K, Nikaido H (2009) Kinetic behavior of the major multidrug efflux pump
673   AcrB of Escherichia coli. Proc Natl Acad Sci U S A 106: 5854-5858.
674   6. Lim SP, Nikaido H (2010) Kinetic parameters of efflux of penicillins by the
675   multidrug efflux transporter AcrAB-TolC of Escherichia coli. Antimicrob
676   Agents Chemother 54: 1800-1806.
677   7. Asuquo AE, Piddock LJ (1993) Accumulation and killing kinetics of fifteen
678   quinolones for Escherichia coli, Staphylococcus aureus and Pseudomonas
679   aeruginosa. J Antimicrob Chemother 31: 865-880.
680   8. Diver JM, Piddock LJ, Wise R (1990) The accumulation of five quinolone
681   antibacterial agents by Escherichia coli. J Antimicrob Chemother 25: 319-333.
682   9. Thanassi DG, Suh GS, Nikaido H (1995) Role of outer membrane barrier in efflux-
683   mediated tetracycline resistance of Escherichia coli. J Bacteriol 177: 998-
684   1007.
685   10. Nikaido H, Thanassi DG (1993) Penetration of lipophilic agents with multiple
686   protonation sites into bacterial cells: tetracyclines and fluoroquinolones as
687   examples. Antimicrob Agents Chemother 37: 1393-1399.
688   11. Demchick P, Koch AL (1996) The permeability of the wall fabric of Escherichia
689   coli and Bacillus subtilis. J Bacteriol 178: 768-773.
690   12. Vazquez-Laslop N, Lee H, Hu R, Neyfakh AA (2001) Molecular sieve mechanism
691   of selective release of cytoplasmic proteins by osmotically shocked
692   Escherichia coli. J Bacteriol 183: 2399-2404.
693   13. Brown S, Santa Maria JP, Jr., Walker S (2013) Wall teichoic acids of gram-positive
694   bacteria. Annu Rev Microbiol 67: 313-336.
695   14. Silhavy TJ, Kahne D, Walker S (2010) The bacterial cell envelope. Cold Spring
696   Harb Perspect Biol 2: a000414.
697   15. Shen LL, Baranowski J, Pernet AG (1989) Mechanism of inhibition of DNA gyrase
698   by quinolone antibacterials: specificity and cooperativity of drug binding to
699   DNA. Biochemistry 28: 3879-3885.
700   16. Neidhardt FC, Umbarger HE (1996) Chemical Composition of *Escherichia coli*. In:
701   Neidhardt FC, Curtiss III R, Ingraham JL, Lin ECC, Low KB et al., editors.
702   *Escherichia coli* and *Salmonella*: Cellular and Molecular Biology. 2 ed.
703   Washington, D. C.: ASM Press.
704   17. Brown DG, May-Dracka TL, Gagnon MM, Tommasi R (2014) Trends and
705   exceptions of physical properties on antibacterial activity for Gram-positive
706   and Gram-negative pathogens. J Med Chem 57: 10144-10161.

31

707   18. Campos M, Surovtsev IV, Kato S, Paintdakhi A, Beltran B, et al. (2014) A constant
708   size extension drives bacterial cell size homeostasis. Cell 159: 1433-1446.
709   19. Sobol' IM (1990) On sensitivity estimation for nonlinear mathematical models.
710   Matematicheskoe Modelirovanie 2: 112-118.
711   20. Sobol' IM (1993) Asymmetric convergence of approximations of the Monte Carlo
712   method. Computational mathematics and mathematical physics 33: 1391-
713   1396.
714   21. Saltelli A, Andres TH, Homma T (1993) Sensitivity Analysis of Model Output - an
715   Investigation of New Techniques. Computational Statistics & Data Analysis
716   15: 211-238.
717   22. Saltelli A, Ratto M, Andres T, Campolongo F, Cariboni J, et al. (2008) Global
718   Sensitivity Analysis: The Primer: John Wiley & Sons.
719   23. Savageau MA (1976) Biochemical systems analysis: a study of function and
720   design in molecular biology. Reading, MA: Addison-Wesley.
721   24. Savageau MA (2013) System design principles. In: Wall ME, editor. Quantitative
722   Biology: From Molecular to Cellular Systems. Boca Raton: Taylor and Francis.
723   pp. 23-49.
724   25. Gustafson P, Srinivasan C, Wasserman L (1995) Local sensitivity analysis.
725   Bayesian Statistics 5: 631-640.
726   26. Oakley JE, O'Hagan A (2004) Probabilistic sensitivity analysis of complex
727   models: a Bayesian approach. J Roy Stat Soc B 66: 751-769.
728   27. Weiss R (1996) An approach to Bayesian sensitivity analysis. J Roy Stat Soc B 58:
729   739-750.
730   28. Vihola M (2012) Robist adaptice Metropolis algorithm with coerced acceptance
731   rate. Stat Comp 22.
732   29. Bratbak G, Dundas I (1984) Bacterial dry matter content and biomass
733   estimations. Appl Environ Microbiol 48: 755-757.
734
735

736

737

738

739   **Figure Captions**

740   Figure 1. Ofloxacin accumulation data (open squares) with model fits (solid lines).

741   A) *E. coli*. B) *P. aeruginosa*. C) *S. aureus*. Each data point is assumed to have the same

742   measurement error, estimated from the maximum values reported for norfloxacin

743   in Ref. [7] (vertical bars)*.* The external drug concentration of 10 mg/L is shown in

744   each panel in ng/mg units (dashed straight lines), converted using the factors

745   derived from the buoyant densities and dry fraction (Methods). The x-axis is plotted

746   using a log scale, reflecting the time sampling of the data.

747

748   Figure 2. Behavior of the model and connection to parameters.

749

750   Figure 3. Global sensitivity analysis results for *E. coli* (A, B); *P. aeruginosa* (C, D); and

751   *S. aureus* (E, F) models. The left panels (A, C, E) show the main effect results, and the

752   right panels (B,D,F) show the total effect results. Color code: a_1 (cyan); a_2 (yellow);

753   β_1 (magenta); β_2 (green); δ (lavender); and τ (red).

754

755   Figure 4. Local sensitivity analysis (LSA) results for A) *E. coli*; B) *P. aeruginosa*; and

756   C) *S. aureus*. Columns correspond to eigenvectors, ordered left to right from the

757   most to the least sensitive, as in Table 3. Rows correspond to parameters, with

758   labels indicated at the left. The strength and sign of the coefficient of each parameter

759   with each eigenvector is indicated using the color code in the legend to the right.

760

761   Figure 5. Bayesian sensitivity analysis for $E.\,coli$. Pairwise parameter PDFs are

33

762   shown using scatter plots in off-diagonal panels; Monte Carlo sampled points

763   illustrate the extent of the PDFs in the space of parameter values indicated on the x-

764   and y-axes. Panels in transposed positions within the grids contain identical

765   information with the x- and y-axes swapped. PDFs for individual parameters are

766   shown on the diagonals using histograms, with the number of counts in each bin

767   (out of 10^6 total samples) indicated on the y-axis.

768   Figure 6. Bayesian sensitivity analysis for *P. aeruginosa*. Plots of posterior PDFs for

769   parameter values and pairwise distributions are as in Fig. 5.

770
771   Figure 7. Bayesian sensitivity analysis for *S. aureus*. Plots of posterior PDFs for

772   parameter values and pairwise distributions as in Fig. 5.

773   Figure S1. Bayesian sensitivity analysis for *E. coli* using a sharpened likelihood

774   function. The analysis and presentation is the same as in Fig. 5, but using a 10-fold

775   lower error value.

776   Figure S2. Bayesian sensitivity analysis for *P. aeruginosa* using a sharpened

777   likelihood function. The analysis and presentation is the same as in Fig. 6, but using

778   a 10-fold lower error value.

779   Figure S3. Bayesian sensitivity analysis for *S. aureus* using a sharpened likelihood

780   function. The analysis and presentation is the same as in Fig. 7, but using a 10-fold

781   lower error value.

782

783

784 **Tables**

785

786 Table 1. Estimated parameter values obtained after fitting the model to data on

787 ofloxacin accumulation in different bacteria.

	a_1 (ng/mg)	a_2 (ng/mg)	β_1 (1/s)	β_2 (1/s)	δ (1/s)	τ (s)
E. coli	32.0	67.1	0.116	0.00125	0.000048	772
P. aeruginosa	7.43	13.7	>0.1[a]	>0.1[a]	0.000314	44.5
S. aureus	66.6	85.2	0.169	0.0014	0.000091	740

788

789 [a]Entries using '>' represent lower bounds.

35

790 Table 2. Parameter ranges used for prior distributions for GSA and BSA (Log_{10}

791 transformed values). Units of parameters are as in Table 1.

	$Log_{10}\, a_1$	$Log_{10}\, a_2$	$Log_{10}\, \beta_1$	$Log_{10}\, \beta_2$	$Log_{10}\, \delta$	$Log_{10}\, \tau$
			E. coli			
min	0	0	-3	-3	-7	0
max	2	2	0	0	-3.5	4
			P. aeruginosa			
min	0	0	-1	-1	-7	0
max	2	2	4	4	-2	4
			S. aureus			
min	0	0	-3	-3	-7	0
max	2	2	0	0	-3.5	4

792

793

794

795

796   Table 3. Sensitivities calculated from eigenvalues corresponding to each eigenvector

797   from LSA. Sensitivity values are calculated as $-\text{Log}_{10}(\lambda)$, where λ is the eigenvalue.

798   The connection of each eigenvector to the model parameters is visualized in Fig. 4.

799

800	Eigenvector #	*E. coli*	*P. aeruginosa*	*S. aureus*
801	1	3.6	3.7	3.6
802	2	3.5	2.7	3.1
803	3	2.4	2.0	1.5
804	4	1.7	-1.9	1.2
805	5	1.3	-6.7	0.5
806	6	-1.0	-11.8	-1.2

37

807   Table 4. Minimum and maximum values of parameters among 10^6 random samples

808   obtained by BSA MCMC (Log$_{10}$ transformed values). Units for parameters are as in

809   Table 1.

	$\text{Log}_{10}\, a_1$	$\text{Log}_{10}\, a_2$	$\text{Log}_{10}\, \beta_1$	$\text{Log}_{10}\, \beta_2$	$\text{Log}_{10}\, \delta$	$\text{Log}_{10}\, \tau$
			E. coli			
min	1.49	1.75	-1.05	-3.00	-7.00	2.81
max	1.52	1.90	-0.80	-2.57	-3.90	2.94
range	0.03	0.14	0.25	0.43	3.10	0.13
			P. aeruginosa			
min	0.76	1.08	-1.00	-1.00	-3.75	1.53
max	0.97	1.18	4.00	4.00	-3.28	1.69
range	0.21	0.10	5.00	5.00	0.47	0.16
			S. aureus			
min	1.82	1.88	-0.84	-3.00	-4.53	2.76
max	1.83	1.98	-0.69	-0.77	-3.80	2.96
range	0.01	0.10	0.15	2.23	0.73	0.20

810

811

812

813   Table 5. Predicted accumulation factors (ϕ), permeabilities (α), and net efflux (ε)

814   rates.

815

	ϕ_1	ϕ_2	α_1 (1/s)	α_2 (1/s)	ε_1 (1/s)	ε_2 (1/s)
E. coli	1.09	2.29	0.126	0.0029	-0.011	-0.0016
P. aeruginosa	0.39	0.72	>0.039[a]	>0.072[a]	>0[a]	>0[a]
S. aureus	2.93	3.75	0.495	0.0053	-0.326	-0.0039

816

817   [a]Entries with a '>' indicate a lower bound.

818

819

820

39
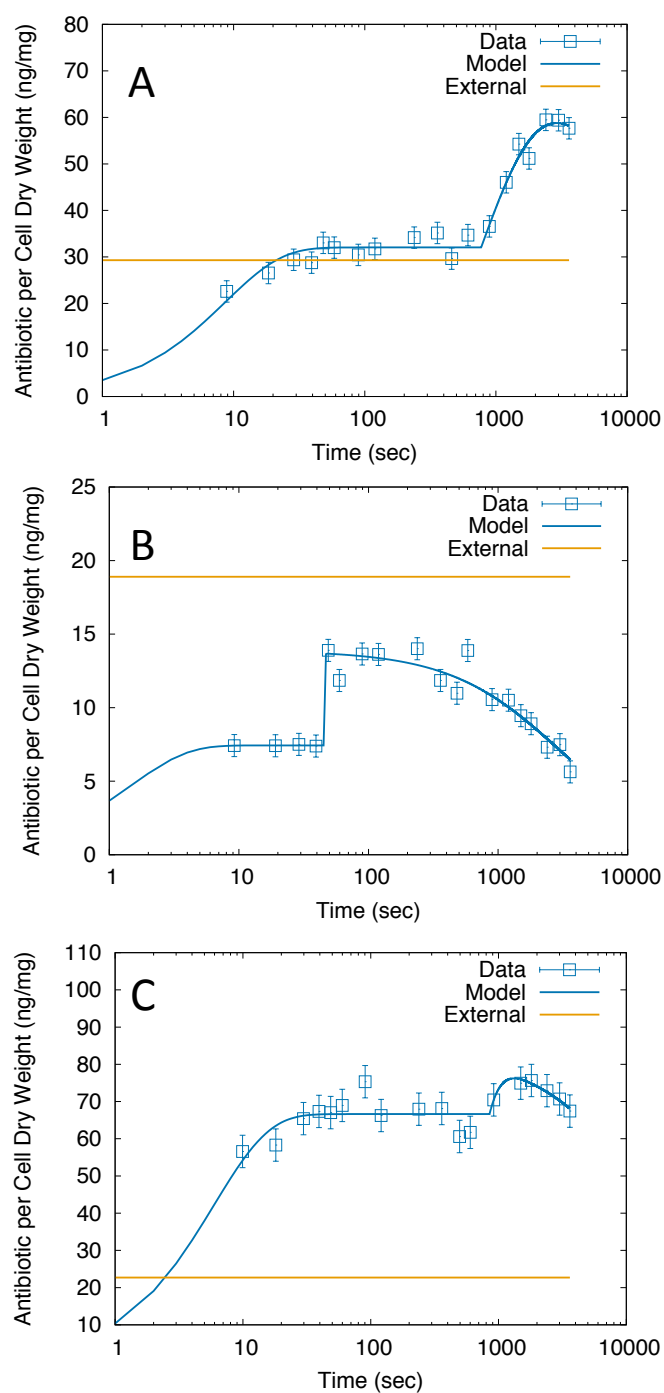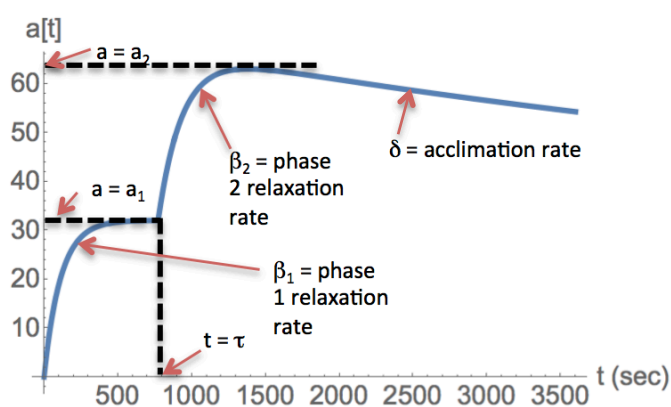
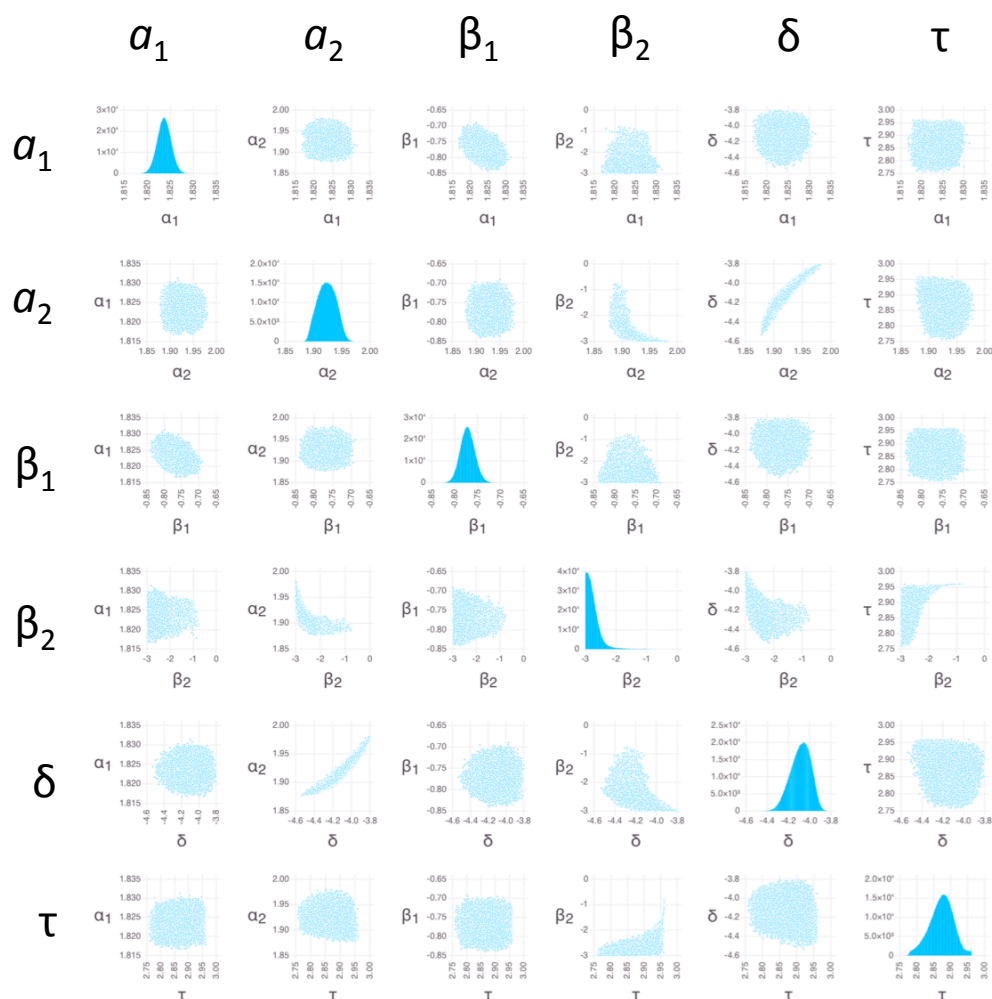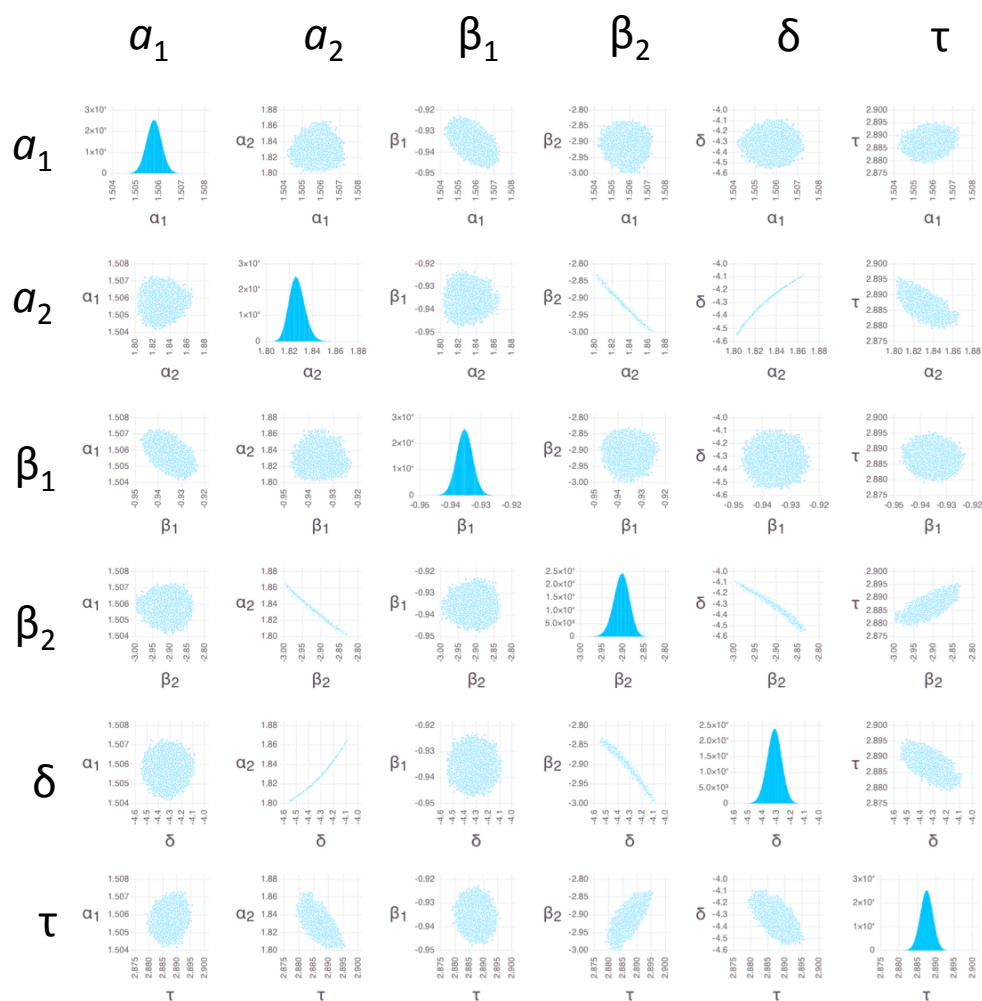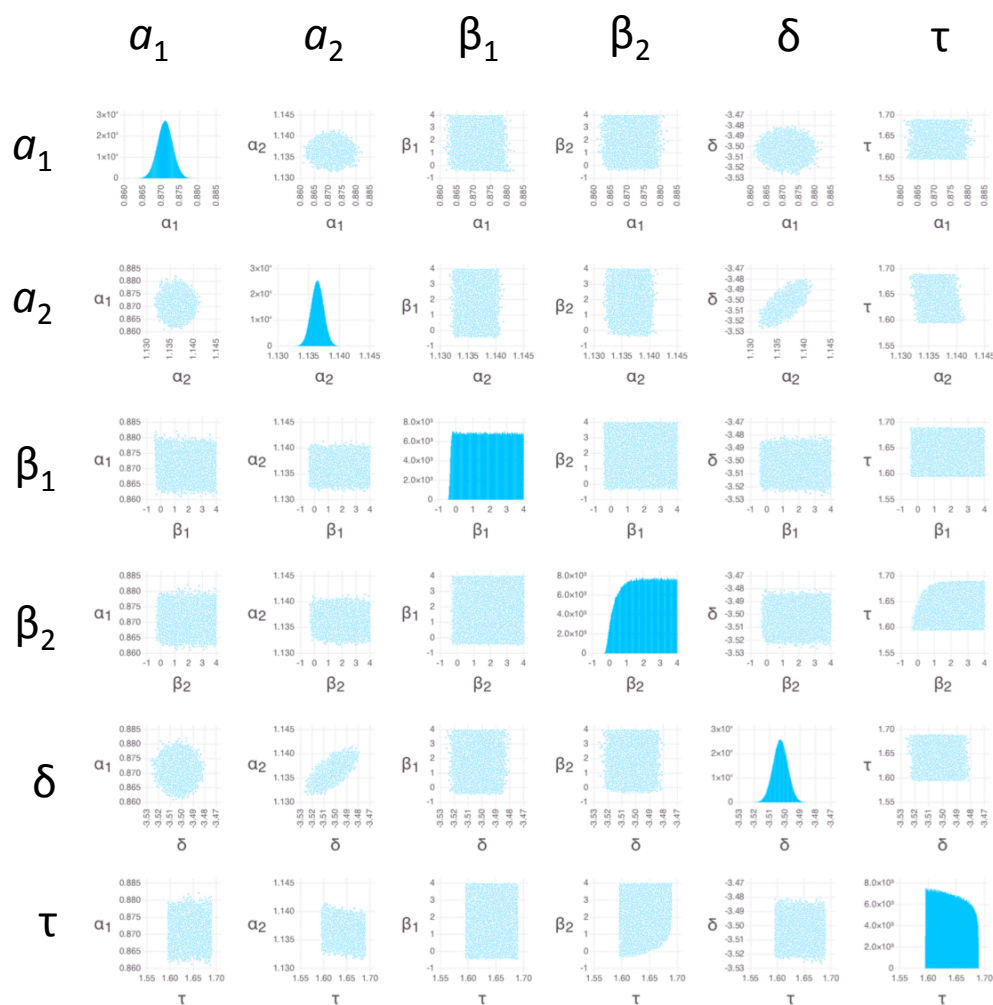# Figure 1

Figure 2

Figure 3
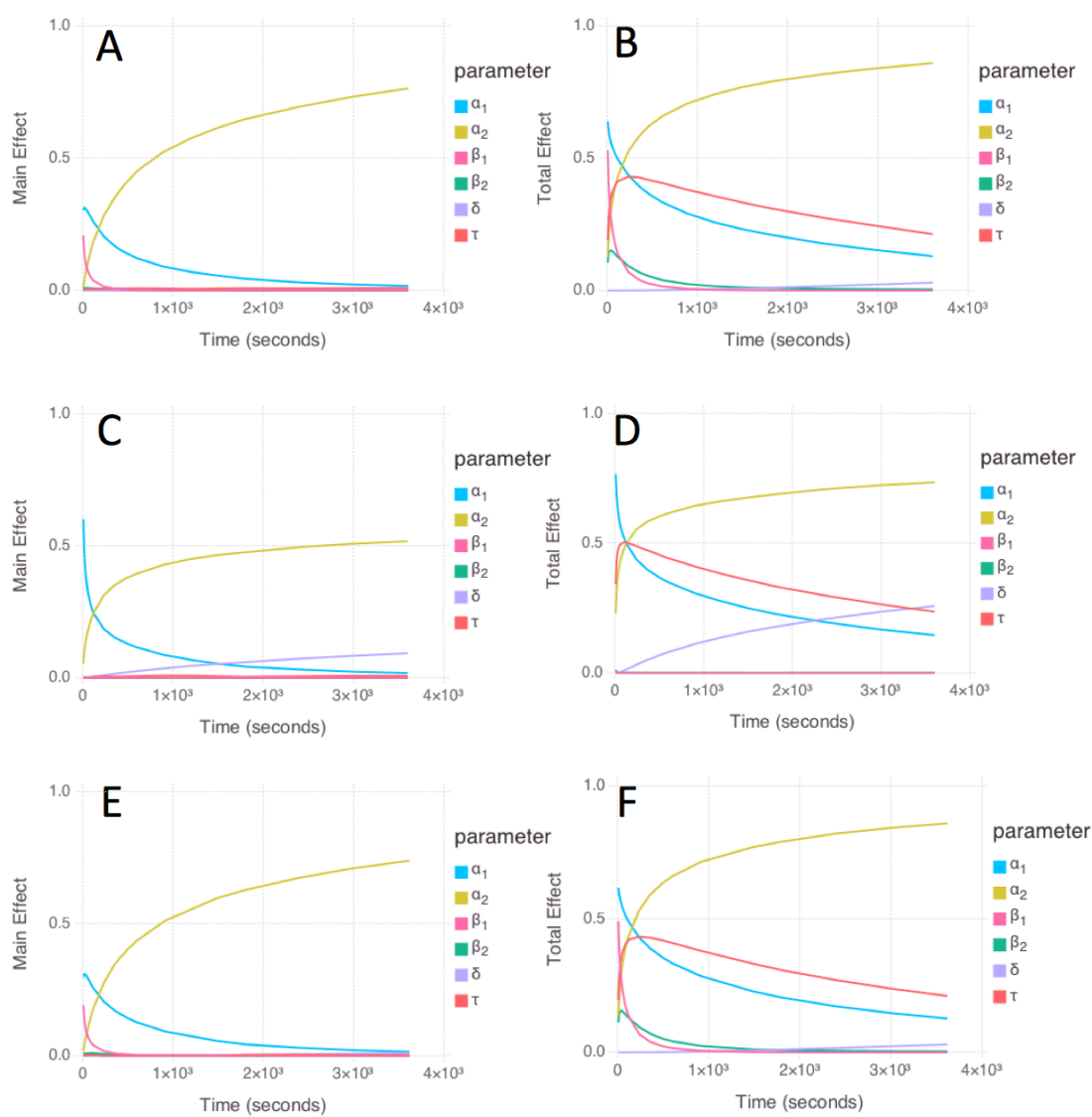
Figure 4
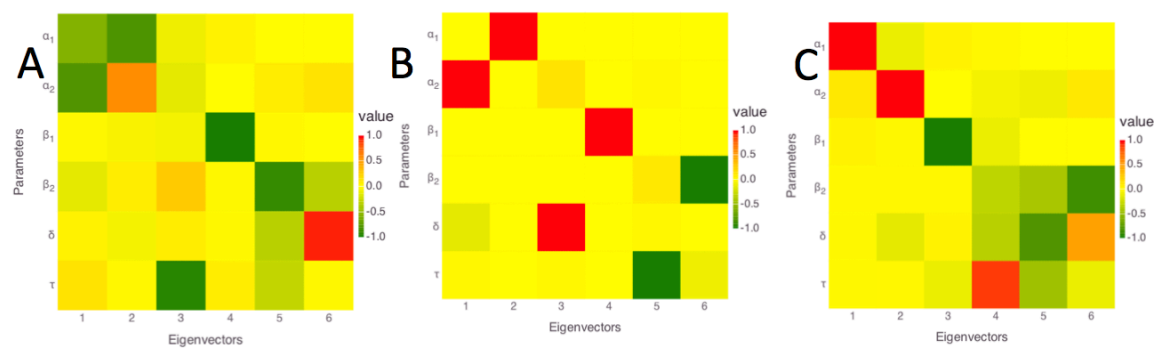
Figure 5
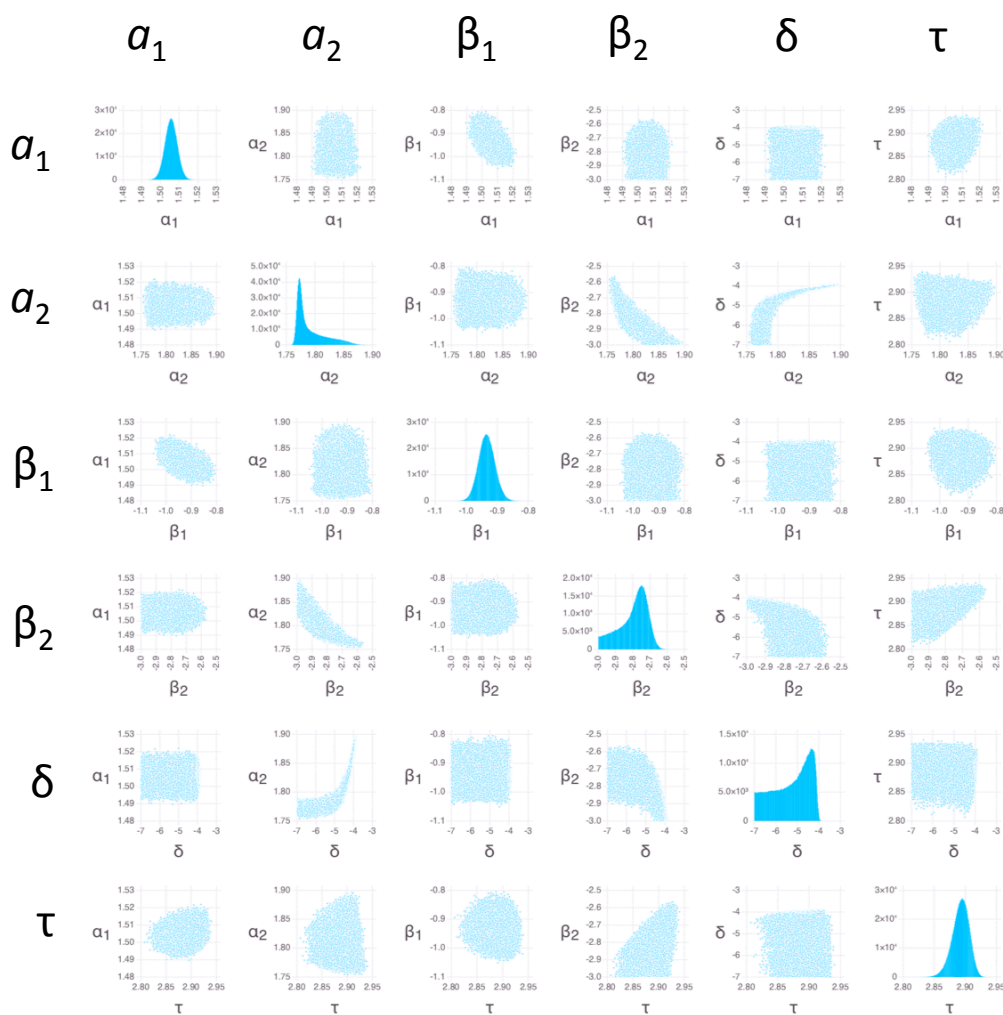
Figure 6
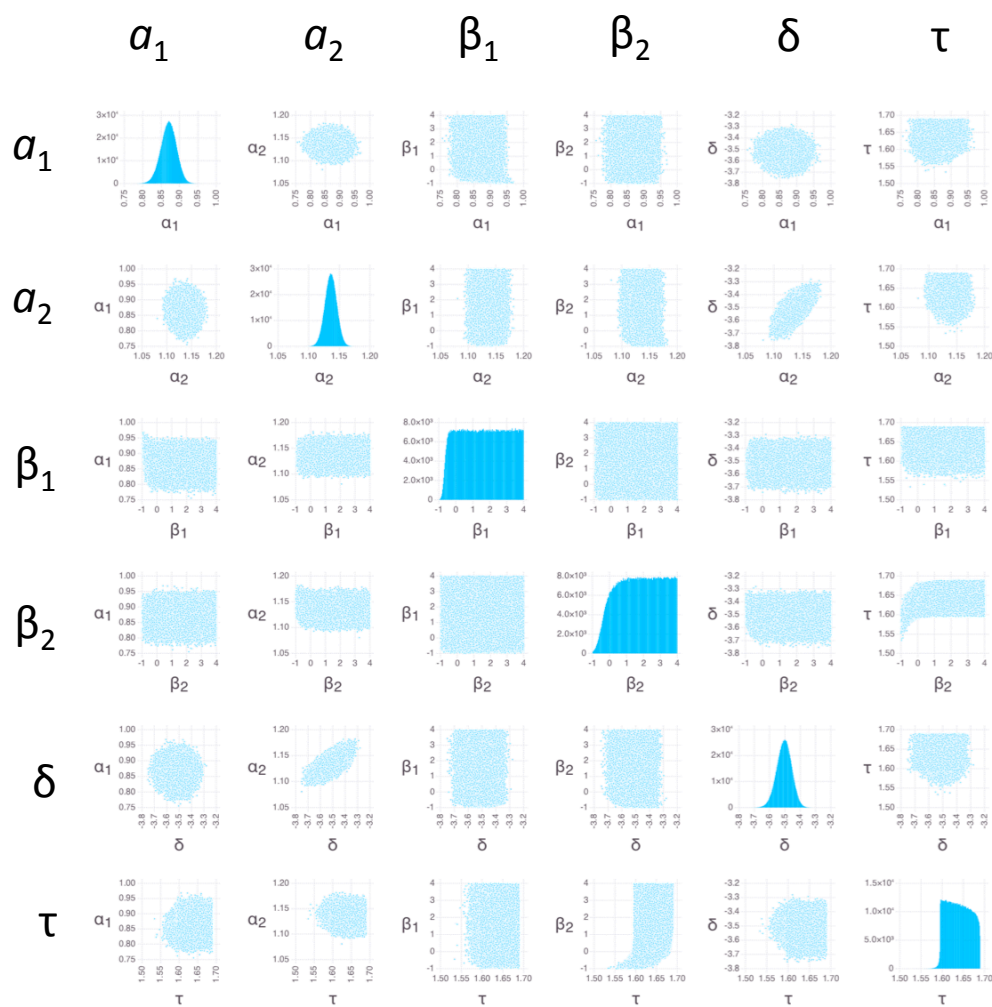
Figure 7

Figure S1

Figure S2

Figure S3